APCTP Pre2015-007, YITP-15-61, RESCEU-22/15

Reheating signature in the gravitational wave spectrum from self-ordering scalar fields

Sachiko Kuroyanagi,[1,2] Takashi Hiramatsu,[3] and Jun'ichi Yokoyama[4,5,6]

[1] *Asia Pacific Center for Theoretical Physics, Pohang, Gyeongbuk 790-784, Korea*
[2] *Department of Physics, Nagoya University, Chikusa, Nagoya 464-8602, Japan*
[3] *Yukawa Institute for Theoretical Physics, Kyoto University, Kyoto 606-8502, Japan*
[4] *Research Center for the Early Universe (RESCEU), School of Science, The University of Tokyo, Tokyo 113-0033, Japan*
[5] *Department of Physics, School of Science, The University of Tokyo, Tokyo 113-0033, Japan*
[6] *Kavli Institute for the Physics and Mathematics of the Universe (Kavli IPMU), The University of Tokyo, Chiba, 277-8568, Japan*

arXiv:1509.08264v1 [astro-ph.CO] 28 Sep 2015

We investigate the imprint of reheating on the gravitational wave spectrum produced by self-ordering of multi-component scalar fields after a global phase transition. The equation of state of the Universe during reheating, which usually has different behaviour from that of a radiation-dominated Universe, affects the evolution of gravitational waves through the Hubble expansion term in the equations of motion. This gives rise to a different power-law behavior of frequency in the gravitational wave spectrum. The reheating history is therefore imprinted in the shape of the spectrum. We perform 512^3 lattice simulations to investigate how the ordering scalar field reacts to the change of the Hubble expansion and how the reheating effect arises in the spectrum. We also compare the result with inflation-produced gravitational waves, which has a similar spectral shape, and discuss whether it is possible to distinguish the origin between inflation and global phase transition by detecting the shape with future direct detection gravitational wave experiments such as DECIGO.

I. INTRODUCTION

Detection of gravitational waves is an exciting new observational frontier in astrophysics and cosmology. Ground-based laser interferometric detectors of new generation, such as Advanced-LIGO [1], Advanced-VIRGO [2] and KAGRA [3], are currently under construction. They promise to yield new insights on many types of astrophysical events. In future, satellite experiments such as eLISA [4, 5], DECIGO [6, 7] and BBO [8] would enable us to explore the Universe with an unprecedented sensitivity at lower frequencies and provide a wealth of important information not only for astronomy, but also for cosmology.

Thanks to the weak interactions with matter, gravitational waves offer a unique opportunity to directly observe the earliest epochs of the Universe beyond the last scattering surface of photons. One interesting source of gravitational waves in the early Universe is a scalar field whose non-vanishing expectation value breaks a global $O(N)$ symmetry [9]. After the phase transition, the self-ordering of the Goldstone modes continuously sources gravitational waves at the horizon scale and produce a scale-invariant spectrum.

Such scale-invariant gravitational waves can be tested by various types of experiments at different frequency bands. While ground-based direct detection experiments have sensitivity at ~ 100Hz, space missions explore gravitational waves at lower frequencies; eLISA will probe $\sim 10^{-3}$Hz; and DECIGO/BBO is designed to measure those at $\sim 0.1 - 1$Hz. There are also indirect means of observations such as B-mode polarization in the Cosmic Microwave Background (CMB) [10–14] and pulsar timing observations [15–18], which can probe gravitational waves at $\sim 10^{-18}$Hz and $\sim 10^{-8}$Hz, respectively.

Several analytical and numerical studies have been conducted to estimate the amplitude of the gravitational wave background from a global phase transition [19–22] and their results are mutually consistent in the large N limit. The effects on CMB have also been studied in the literature, in terms of temperature and polarization anisotropies [23–25], non-Gaussianity [27, 30] and spectral distortions [28]. The difference from the inflationary gravitational wave background, which also has a nearly scale-invariant spectrum, has been studied in [29–31] focusing on the CMB scale. Recently, the Planck satellite has placed an upper limit on the effective defect energy scale of global textures, $G\mu < 1.1 \times 10^{-6}$ [32], where G is Newton's constant. The energy scale μ is related with the vacuum expectation value of the $O(4)$ scalar fields, v, as $\mu = \pi v^2$. [1] In terms of v, the constraint is rewritten as $v/m_{\rm pl} < 6 \times 10^{-4}$ with $m_{\rm pl} = G^{-1/2} = 1.2 \times 10^{19}$ GeV being the Planck scale. The contribution on the B-mode polarization signal has also been studied motivated by the BICEP2 experiment [34, 35] and a slightly better constraint is obtained,

[1] Note that the relation between μ and v is different from the Planck paper by a factor of 2, because we adopt a Lagrangian of real scalar fields in this paper, while the Planck paper uses the Lagrangian of complex scalar fields. For details see the appendix in Ref. [33].

$G\mu < 7.3 \times 10^{-7}$ [36], which corresponds to $v/m_{\rm pl} < 5 \times 10^{-4}$. Since the peak of the signal in the B-mode spectrum arises at different scale, the constraint on gravitational waves from a global $O(N)$ phase transition is weaker compared to that of inflation.

The purpose of this paper is to investigate the effect of reheating on the gravitational wave spectrum of a global $O(N)$ phase transition, and make a prediction for future direct detection experiments. It is known that the Hubble expansion rate of the Universe makes difference in the power of generated gravitational waves [19, 31]. It also affects the decline rate of the amplitude due to redshift after generation. After the phase transition, gravitational waves are continuously generated as the random initial configuration of the scalar field is homogenized up to the Hubble horizon scale at each epoch, and information of expansion rate is contained in the spectral amplitude of the mode. In the ordinary scenario of reheating, the Universe is dominated by the coherently oscillating inflaton field with a quadratic inflaton potential, which results in the same expansion rate as that of the matter-dominated Universe. When reheating is completed, the Universe becomes radiation-dominated. Therefore, information on the transition of the expansion rate at the end of reheating may be imprinted in the gravitational waves generated around the completion of reheating. The corresponding frequency of the gravitational wave spectrum is related to the energy scale of reheating.

A similar effect arises in the spectrum of the inflationary gravitational wave background. Interestingly, it has been shown that the effect arises in the sensitivity range of DECIGO and BBO, if the energy scale of reheating, or similar mechanism to yield a matter-dominated early Universe such as a late-time entropy production, is around 10^7GeV [37–44]. The same would be expected in the case of a global $O(N)$ phase transition, and could be explored by those experiments.

In this paper, we perform lattice simulations to explicitly evaluate the effect of reheating on the gravitational wave spectrum. While inflationary gravitational waves are generated when each mode crosses outside the Hubble horizon during inflation, in the case of the $O(N)$ phase transition, gravitational waves are sourced by the anisotropic stress of the scalar field when the mode enters the horizon after the phase transition. Because of the difference in the generation process, the effect of reheating arises in a different way. To obtain the gravitational wave spectrum, we follow the evolution of both the scalar field and gravitational wave in a 3-dimensional lattice with changing the background equation of state. Lattice simulations provide an accurate estimate including non-linear dynamics of the scalar field.

The paper is organized as follows. In the next section, we describe background equations during reheating, and the evolution equations of the scalar field and gravitational waves, used in the lattice simulations. In Sec. III, we show the spectra obtained from our simulations. Then we discuss the differences between the spectrum from the $O(N)$ phase transition and that from inflation. Furthermore, we perform a Fisher matrix analysis and investigate whether we can determine the reheating temperature by observing the reheating signature in the spectrum with future experiments such as DECIGO and Ultimate DECIGO. We also discuss if we can determine the origin of the observed gravitational wave background by measuring the small differences between inflation and $O(N)$ phase transition origin. Section IV is devoted to conclusion.

II. MODEL

In this section, we describe setup for our simulation. For the background, we assume the conventional reheating scenario in which the inflaton energy is transferred to the radiation energy while the inflaton oscillates around the bottom of its quadratic potential. The inflaton energy is the dominant component during the reheating phase and the expansion rate is the same as the matter-dominated Universe. As the energy-transfer process proceeds, the Universe becomes radiation-dominated.

Under this background, we consider a phase transition, where the global $O(N)$ symmetry of a scalar field is broken to $O(N-1)$. The field rolls down to the true vacuum when the symmetry is broken, and each causally disconnected region of the Universe gets arbitrarily different directions of the field, which yields the spatial gradient of the field on superhorizon scales. As the comoving Hubble horizon grows, previously causally disconnected regions come into contact and the field moves to match the orientation, which is called self-ordering. The field releases gradient energy as it relaxes and generates anisotropic stresses that source gravitational waves.

We consider the case where the symmetry breaking occurs well before the universe becomes radiation dominated, so that the information on the transition from matter- to radiation-dominated phase is imprinted on the gravitational wave spectrum.

A. Background equations for the reheating process

We work in a spatially flat Friedmann-Lemaître-Robertson-Walker background with the metric

$$ds^2 = a^2(\tau)(-d\tau^2 + \delta_{ij}dx^i dx^j), \tag{1}$$

where τ denotes conformal time and $a(\tau)$ is the scale factor. For the reheating process, we assume a perturbative decay of the inflaton field φ into radiation. Assuming that the inflaton potential U is approximated as $U = m^2\varphi^2/2$ during the oscillating phase, the equation for the energy density of the scalar field is given by

$$\rho'_\varphi + 3\mathcal{H}\rho_\varphi = -a\Gamma\rho_\varphi, \tag{2}$$

where $\rho_\varphi = \varphi'^2/(2a^2) + U$, Γ is the decay rate of φ and the prime denotes the derivative with respect to τ. This has an analytic solution $\rho_\varphi \propto a^{-3}\exp(-\Gamma t)$, where t denotes cosmic time $dt = ad\tau$. Assuming that all the decay products of the inflaton are rapidly thermalized, the energy conservation equation of radiation density reads

$$\rho'_r + 4\mathcal{H}\rho_r = a\Gamma\rho_\varphi. \tag{3}$$

The expansion rate of the Universe, $\mathcal{H} \equiv a'/a$, is determined by the sum of the energy densities,

$$\mathcal{H}^2 = \frac{a^2}{3M_{\rm pl}^2}(\rho_\varphi + \rho_r), \tag{4}$$

where $M_{\rm pl} = (8\pi G)^{-1/2}$ is the reduced Planck scale. We numerically solve these three equations, Eqs. (2) – (4), to calculate the Hubble expansion rate in our simulation, although they admit the following analytic solution

$$\rho_\phi(t) = \rho_\phi(t_i)\left[\frac{a(t)}{a(t_i)}\right]^{-3} e^{-\Gamma(t-t_i)} \tag{5}$$

$$\rho_r(t) = \Gamma\int_{t_i}^{t}\left[\frac{a(t)}{a(t')}\right]^{-3}\rho_\phi(t')dt', \tag{6}$$

which is valid if $\rho_r(t_i)$ is negligible. For $t_i \ll t \ll \Gamma^{-1}$ (6) can be expressed as

$$\rho_r(t) = \frac{3}{5}\Gamma t\left[\frac{a(t)}{a(t_i)}\right]^{-3}\rho_\phi(t_i) \cong \frac{6}{5}\Gamma H M_{\rm pl}^2, \tag{7}$$

with $H = \mathcal{H}/a$. The temperature of the Universe is therefore given by

$$T = \left(\frac{30}{\pi^2 g_*}\rho_r\right)^{\frac{1}{4}} \simeq \left(\frac{36}{\pi^2 g_*}\Gamma H M_{\rm pl}^2\right)^{\frac{1}{4}}, \tag{8}$$

where g_* is the effective number of relativistic degrees of freedom. The universe becomes radiation dominant at $t \simeq \Gamma^{-1}$. The temperature at this time, the reheating temperature, is determined using this relation as

$$T_{\rm RH} \simeq \left(\frac{10}{\pi^2 g_*}\right)^{\frac{1}{4}}(M_{\rm pl}\Gamma)^{\frac{1}{2}}. \tag{9}$$

B. Global O(N) symmetric scalar field model

We consider an N-component real scalar field $\Phi = (\phi_1, \phi_2, ..., \phi_a, ..., \phi_N)$ with a Lagrangian

$$\mathscr{L}(\Phi) = -\frac{1}{2}(\partial_\mu\Phi)^T(\partial^\mu\Phi) - V_{\rm eff}(\Phi, T), \tag{10}$$

with a temperature-dependent effective potential [45]

$$V_{\rm eff}(\Phi, T) = \frac{\lambda}{2}(\Phi^2 - v^2)^2 + \frac{\lambda}{3}T^2\Phi^2, \tag{11}$$

where $\Phi^2 = \sum_a \phi_a^2$, λ is the dimensionless self-coupling of Φ, and v is the magnitude of the vacuum expectation value in the true vacuum. Throughout the paper, we take $\lambda = 1$. The symmetry is broken below the critical temperature $T_c = \sqrt{3}v$. After symmetry breaking, the scalar field acquires a vacuum expectation value and satisfies $\Phi^2 = v^2$.

The equations of motion for each component of the scalar field is given by

$$\phi_a''(\tau, \boldsymbol{x}) + 2\mathcal{H}\phi_a'(\tau, \boldsymbol{x}) - \nabla^2\phi_a(\tau, \boldsymbol{x}) = -a^2\frac{\partial V_{\rm eff}}{\partial \phi_a}. \tag{12}$$

In order to set the initial condition without ambiguities we assume that the symmetry is restored by high-temperature effects after inflation characterized by (8) and start simulations from a symmetric state. To realize the initial condition, we generate zero-mean Gaussian random values for $\widetilde{\phi}_a(t_0, \boldsymbol{k})$ and $\dot{\widetilde{\phi}}_a(t_0, \boldsymbol{k})$ on a discrete grid in the Fourier space with the variance [45, 46],

$$\langle|\widetilde{\phi_a}(t_0, \boldsymbol{k})|^2\rangle = VP(\tau_0, |\boldsymbol{k}|), \quad \langle|\dot{\widetilde{\phi}}_a(t_0, \boldsymbol{k})|^2\rangle = VQ(\tau_0, |\boldsymbol{k}|), \tag{13}$$

with

$$P(\tau, k) = \frac{1}{\omega_k}\frac{1}{e^{\beta_T\omega_k} - 1}, \quad Q(\tau, k) = \frac{\omega_k}{e^{\beta_T\omega_k} - 1}, \tag{14}$$

where $\omega_k = \sqrt{k^2 + m^2}$ with $m^2 = d^2V_{\rm eff}/d\Phi^2|_{\Phi=0}$ being the effective mass of the scalar field, $\beta_T = 1/T$ and $V = L^3$ is the comoving volume of the simulation box. Note that here we use the proper time t instead of τ and the dot denotes the derivative with respect to t. Then, transforming $\widetilde{\phi}_a$ and $\dot{\widetilde{\phi}}_a$ to the real space, $\phi_a(\tau_0, \boldsymbol{x})$ and $\dot{\phi}_a(\tau_0, \boldsymbol{x})$ have the desired thermal distribution.

C. Gravitational waves

Gravitational waves are represented by a transverse-traceless gauge-invariant metric perturbation, h_{ij}, in a Friedmann Robertson-Walker background.

$$ds^2 = a^2(\tau)\left[-d\tau^2 + (\delta_{ij} + h_{ij})dx^i dx^j\right], \tag{15}$$

where h_{ij} satisfies $h^{ij}{}_{,j} = h^i{}_i = 0$. Expanding the Einstein equations to first order in h_{ij}, we obtain the equation of motion

$$h_{ij}''(\tau, \boldsymbol{x}) + 2\mathcal{H}h_{ij}'(\tau, \boldsymbol{x}) - \nabla^2 h_{ij}(\tau, \boldsymbol{x}) = \frac{2}{M_{\rm pl}^2}\Pi_{ij}^{\rm TT}(\tau, \boldsymbol{x}), \tag{16}$$

where the source term, $\Pi_{ij}^{\rm TT}(\tau, \boldsymbol{x})$ is the transverse-traceless projection of the anisotropic stress tensor,

$$\Pi_{ij}(\tau, \boldsymbol{x}) = \sum_a\left[\partial_i\phi_a(\tau, \boldsymbol{x})\partial_j\phi_a(\tau, \boldsymbol{x}) - \frac{1}{3}\delta_{ij}\partial_k\phi_a(\tau, \boldsymbol{x})\partial^k\phi_a(\tau, \boldsymbol{x})\right]. \tag{17}$$

The transverse-traceless part is obtained by applying the projection operator in the momentum space

$$\Pi_{ij}^{\rm TT}(\tau, \boldsymbol{k}) = \Lambda_{ij,k\ell}(\hat{k})\Pi_{k\ell}(\tau, \boldsymbol{k}) = \Lambda_{ij,k\ell}(\hat{k})\sum_a\{\partial_k\phi_a\partial_\ell\phi_a\}(\tau, \boldsymbol{k}), \tag{18}$$

with

$$\Lambda_{ij,k\ell}(\hat{k}) = \mathcal{P}_{ik}(\hat{k})\mathcal{P}_{j\ell}(\hat{k}) - \frac{1}{2}\mathcal{P}_{ij}(\hat{k})\mathcal{P}_{k\ell}(\hat{k}), \tag{19}$$

$$\mathcal{P}_{ij}(\hat{k}) = \delta_{ij} - \hat{k}_i\hat{k}_j, \tag{20}$$

where $\{\partial_k\phi_a\partial_\ell\phi_a\}(\tau, \boldsymbol{k})$ denotes the Fourier transform of $\partial_k\phi_a(\tau, \boldsymbol{x})\partial_\ell\phi_a(\tau, \boldsymbol{x})$ and $\hat{k} = \boldsymbol{k}/k$ [47].

III. LATTICE SIMULATION

A. Set up

In order to calculate the gravitational wave spectrum, we perform lattice simulations by numerically evolving the scalar field and gravitational wave on a discrete lattice. Introducing new variables ψ_a and χ_{ij} defined as $\phi_a = \psi_a/a$ and $h_{ij} = \Lambda_{ij,k\ell}\chi_{k\ell}/a$, we solve the following equations

$$\psi_a''(\tau,\boldsymbol{x}) - \frac{a''}{a}\psi_a(\tau,\boldsymbol{x}) - \nabla^2\psi_a(\tau,\boldsymbol{x}) = -2\lambda a^2\left(\Phi^2 - v^2 + \frac{T^2}{3}\right)\psi_a(\tau,\boldsymbol{x}), \tag{21}$$

$$\chi_{ij}''(\tau,\boldsymbol{x}) - \frac{a''}{a}\chi_{ij}(\tau,\boldsymbol{x}) - \nabla^2\chi_{ij}(\tau,\boldsymbol{x}) = \frac{2}{M_{\rm pl}^2 a}\sum_a\left[\partial_i\psi_a(\tau,\boldsymbol{x})\partial_j\psi_a(\tau,\boldsymbol{x})\right]. \tag{22}$$

The energy density of the gravitational waves is given by

$$\rho_{\rm GW}(\tau) = \frac{M_{\rm pl}^2}{4a^2}\langle h_{ij}'(\tau,\boldsymbol{x})h_{ij}'(\tau,\boldsymbol{x})\rangle_V = \frac{M_{\rm pl}^2}{4a^4}\frac{1}{V}\int\frac{d^3k}{(2\pi)^3}\left[\Lambda_{ij,kl}(\hat{k})\chi_{kl}'(\tau,\boldsymbol{k})\right]^2, \tag{23}$$

where $\langle\cdots\rangle_V$ represents the average over the spatial volume and $\chi_{ij}(\tau,\boldsymbol{k})$ is the Fourier transform of $\chi_{ij}(\tau,\boldsymbol{x})$. It is commonly parameterized by the dimensionless density parameter per logarithmic frequency interval,

$$\Omega_{\rm GW}(k) \equiv \frac{1}{\rho_c}\frac{d\rho_{GW}}{d\log k}, \tag{24}$$

where ρ_c is the critical density of the Universe, $\rho_c = 3M_{\rm pl}^2\mathcal{H}^2/a^2$. By substituting Eq. (23) into (24), we obtain

$$\Omega_{\rm GW}(k,\tau) = \frac{k^3}{96\pi^3\mathcal{H}^2a^2V}\int d\Omega\,\chi_{ij}'(\tau,\boldsymbol{k})\chi_{ij}'^*(\tau,\boldsymbol{k}), \tag{25}$$

where $d\Omega$ is the integral over the solid angle. Using $\rho_{\rm rad} \propto g_*^{-1/3}a^{-4}$ and $\rho_{\rm GW} \propto a^{-4}$, the energy spectrum at the present time is related to that at the end of simulation as

$$\Omega_{{\rm GW},0}(k) = \Omega_{{\rm rad},0}\left(\frac{g_{*,0}}{g_{*,f}}\right)^{1/3}\Omega_{{\rm GW},f}(k), \tag{26}$$

in the plateau region where gravitational waves are generated after the entropy production from the inflaton has been terminated. Here the subscript 0 denotes the value at the present time and f denotes the value at the end of simulation. Using entropy conservation, $g_*T^3 \propto a^{-3}$, the physical wavenumber at the end of simulation $k_{{\rm phys},f}$ is related to the frequency today as

$$f_0 = \frac{k_{{\rm phys},f}}{2\pi}\frac{a_f}{a_0} = \frac{k_{{\rm phys},f}}{2\pi}\left(\frac{g_{*,0}}{g_{*,f}}\right)^{1/3}\left(\frac{T_0}{T_f}\right). \tag{27}$$

We perform simulations with 512^3 lattices assuming $v = 9\times10^{-4}m_{\rm pl}$, $g_{*,f} = 1000$ and $\Gamma = 0.2v$, which corresponds to $T_{\rm RH} = 2.2\times10^{16}$GeV. The simulation starts before the phase transition. We take the initial scale factor to be $a_{\rm init} = 1$ and the initial Hubble size to be $\mathcal{H}_{\rm init} = 1.1v$, which relates to the conformal time as $\tau_{\rm init} = 2/\mathcal{H}_{\rm init} = 1.8/v$. The simulation stops when the comoving Hubble radius becomes a half of the box size, $\mathcal{H}_{\rm end}^{-1} = L/2$. Then the result is converted to the present value using Eqs. (26) and (27) with $g_{*,0} = 3.36$, $\Omega_{{\rm rad},0}h^2 = 4.15\times10^{-5}$ and $T_0 = 2.725$K, where $h = 0.7$ is the reduced Hubble parameter.

Note that we take a value of v larger than the current CMB constraint and a nonstandard value of g_* in our simulations. Furthermore the initial value of the Hubble parameter at the beginning of simulations also exceeds the constraints on the Hubble parameter imposed by the tensor perturbations generated during standard inflation, although we can evade such a constraint if we adopt an inflation model in which the null energy condition is violated [48]. The reason why we choose such nonstandard values of v an g_* is that, for small values of v and g_*, gravitational waves generated by self-ordering scalar fields after the phase transition are contaminated by those generated from the thermal fluctuations of the scalar fields before the transition. In order to suppress this contamination and focus on the effect from reheating, we use relatively large values of v and g_*. In fact, large v enhances the power of gravitational wave spectrum from self-ordering with the dependence of $\Omega_{\rm GW} \propto v^4$, and large g_* reduces the initial temperature and gives smaller thermal fluctuations before the phase transition (see Eqs. (8) and (14) for the temperature dependence of the thermal fluctuations).

Once simulations with such parameters are performed we can obtain results with other parameter values using the above mentioned scaling law $\Omega_{\rm GW} \propto v^4$ as well as other scaling discussed below.

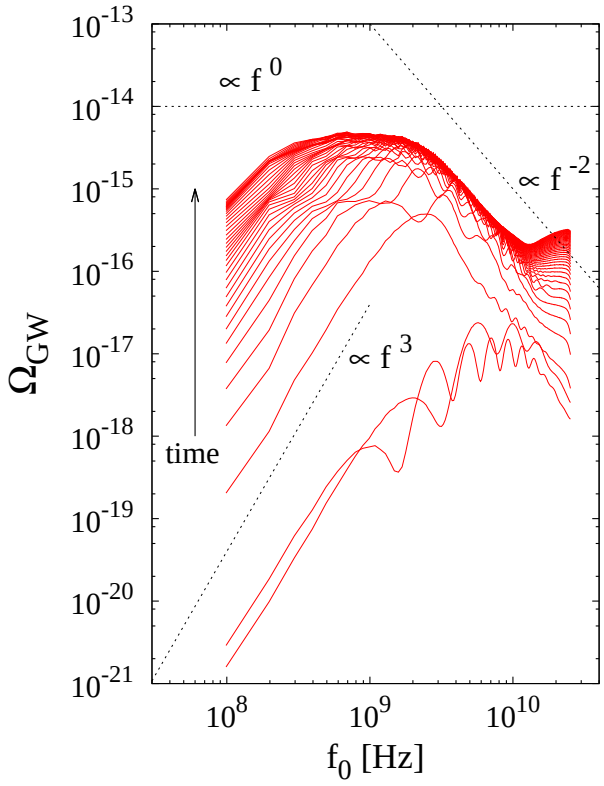

FIG. 1: The gravitational wave spectrum shown in terms of the present gravitational frequency f_0[Hz]. Time evolution is shown from bottom to top. The number of the field component is $N = 4$. The decay rate is taken to be $\Gamma = 0.2v$, which corresponds to $T_{\rm RH} = 2.2 \times 10^{16}$GeV.

B. Results

Figure 1 shows time evolution of the gravitational wave spectrum. We see that higher-frequency modes come inside the horizon earlier and the gravitational wave is generated soon after the mode comes into the horizon. The modes outside the horizon have frequency dependence of f^3, which matches the analytical prediction of Refs. [19, 25]. Note that the f^3 dependence remains in the final spectrum at the lowest frequencies, since we stop the simulation when the Hubble radius becomes half the box size. However, if we could trace the time evolution longer, the f^0 dependence would continue toward the lower frequencies. For the modes inside the horizon at the end of simulation, we see the frequency dependence of the spectrum changes from f^{-2} to f^0 because of the transition from the matter-dominated to the radiation-dominated phase.

The bump seen at the highest frequencies in the final regime of the simulation is an artifact due to the finite resolution (see also Fig. 2). Gravitational waves are not produced if the mode is already inside the horizon at the time of the phase transition. In Fig. 2, we show spectra for smaller box sizes which give a better resolution. We confirm that the spectrum represented in red keeps the initial shape and thus damps exponentially at high frequencies where the bumps appear in the computations with a worse resolution (blue and green).

Figure 3 shows the spectra in the case with different numbers of the scalar field components. Note that the vertical axis is the power multiplied by N. The amplitude of the spectrum has the same dependence with the analytical prediction $\Omega_{\rm GW} \propto 1/N$ [19, 25] for large N. Contrarily, we find the extra power for small N, which would imply the breakdown of the large N approximation used in the analytical predictions. This point has been studied in Ref. [22] and our result is consistent with them.

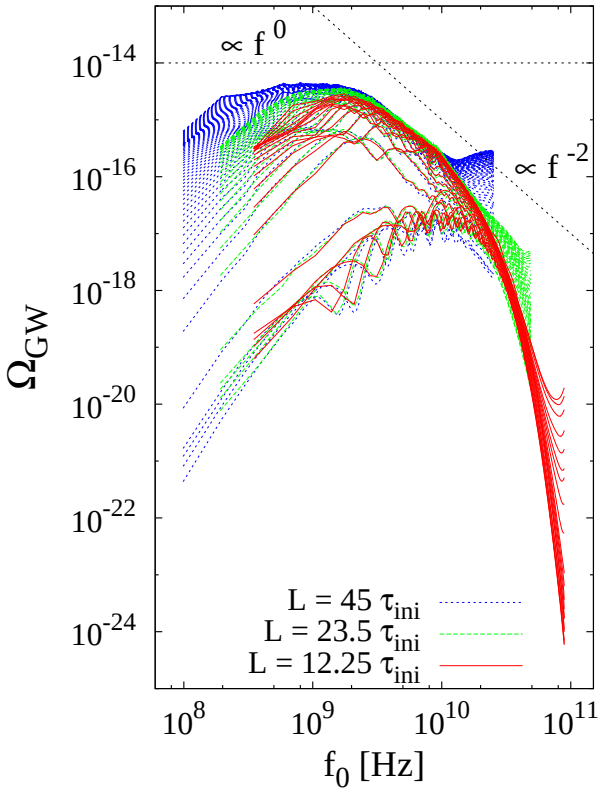

FIG. 2: The gravitational wave spectra for different simulation box sizes. The number of the field component is fixed to be $N = 4$.

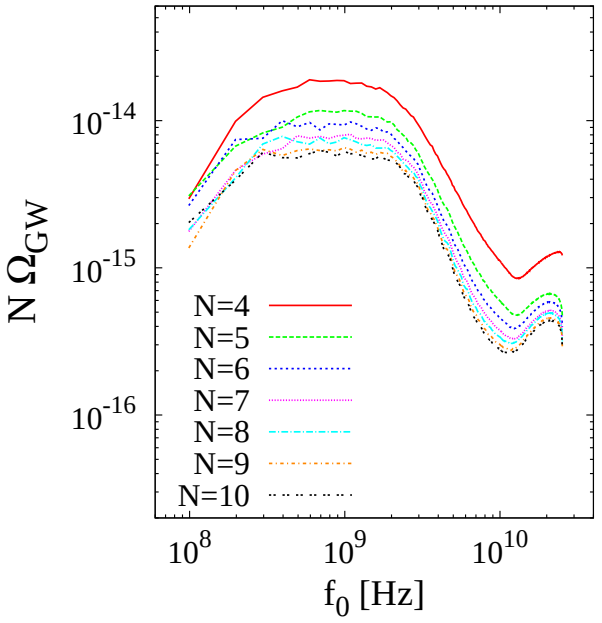

FIG. 3: The gravitational wave spectra for different values of N. The vertical axis is multiplied by N to test the analytically predicted dependence of $\Omega_{\rm GW} \propto 1/N$.

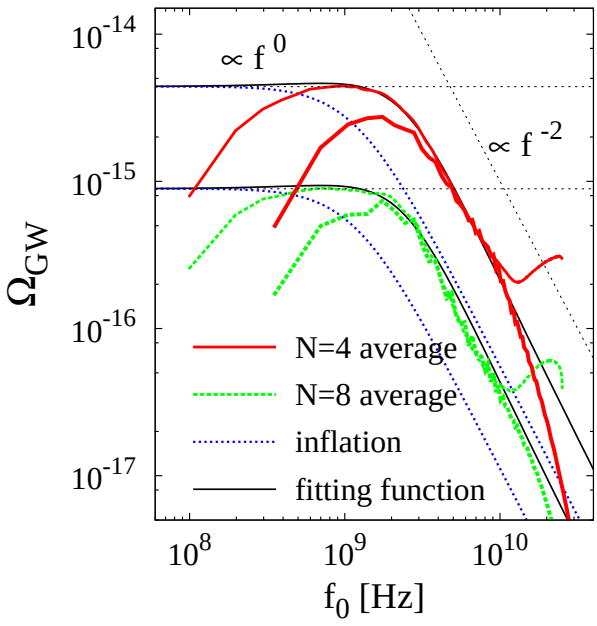

FIG. 4: The gravitational wave background spectra compared with that from inflation. The red solid lines represent the case of $N = 4$ and the green dashed lines represent $N = 8$, while blue dotted lines are the spectra from inflation calculated assuming the same reheating temperature. The decay rate is taken to be $\Gamma = 0.2v$ for all cases, which corresponds to $T_{\rm RH} = 2.2 \times 10^{16}$GeV. For the spectra of $O(N)$ phase transition, we show the averaged values of 20 realizations of simulations with a large box size $L = 45\tau_{\rm ini}$ and a small box size $L = 12.25\tau_{\rm ini}$. For the inflationary gravitational waves, we assume no tilt of the spectrum and the amplitude is tuned to be the same as that of $O(N)$ phase transition spectra at the frequencies where the spectrum has the f^0 dependence. We also show the fitting function, given by Eqs. (28) and (30).

C. Comparison with inflationary gravitational wave spectrum

In Fig. 4, we compare the spectrum with that from inflation. For the spectrum from the $O(N)$ phase transition, we show the spectrum obtained by averaging over 20 realizations of simulation for each combination of parameters. As explained before, the damping of the power seen at the low frequencies is because of the limitation in the simulation time. The f^0 dependence therefore should continue to the lower frequencies. For the spectrum from inflation, we normalized the amplitude at low frequencies and take the value to be the same as the case of the $O(N)$ phase transition for comparison. We also assume the same reheating temperature for both cases.

Comparing the two spectra, we find that there is a difference in the position of the spectral bend. This is because gravitational waves are continuously generated even after the inward horizon crossing until each k mode of scalar field fluctuations is homogenized. We also find that the sharpness of the transition from f^{-2} to f^0 is slightly different around the bend.

Let us introduce a fitting formula to describe the shape of the spectrum caused by reheating and approximate the spectrum as

$$\Omega_{\rm GW}(f) = \Omega_{\rm GW,A} T^2(x_R), \tag{28}$$

where $\Omega_{\rm GW,A}$ is the normalization of the spectral amplitude and $T^2(x_R)$ is the transfer function which describes the transition from f^0 to f^{-2}. For inflation, the transfer function has been found as [49]

$$T^2_{\rm inflation}(x_R) = \left(1 - 0.22 x_R^{1.5} + 0.65 x_R^2\right)^{-1}, \tag{29}$$

where $x_R = f/f_R$ and $f_R = 0.26\,(g_{*s}(T_R)/106.75)^{1/6}\,\left(T_R/10^7\ {\rm GeV}\right){\rm Hz}$. For the $O(N)$ phase transition, we find that the spectrum is well described by the transfer function

$$T^2_{O(N)}(x_{R'}) = \left(1 - 0.6 x_{R'}^{1.5} + 0.65 x_{R'}^2\right)^{-1}, \tag{30}$$

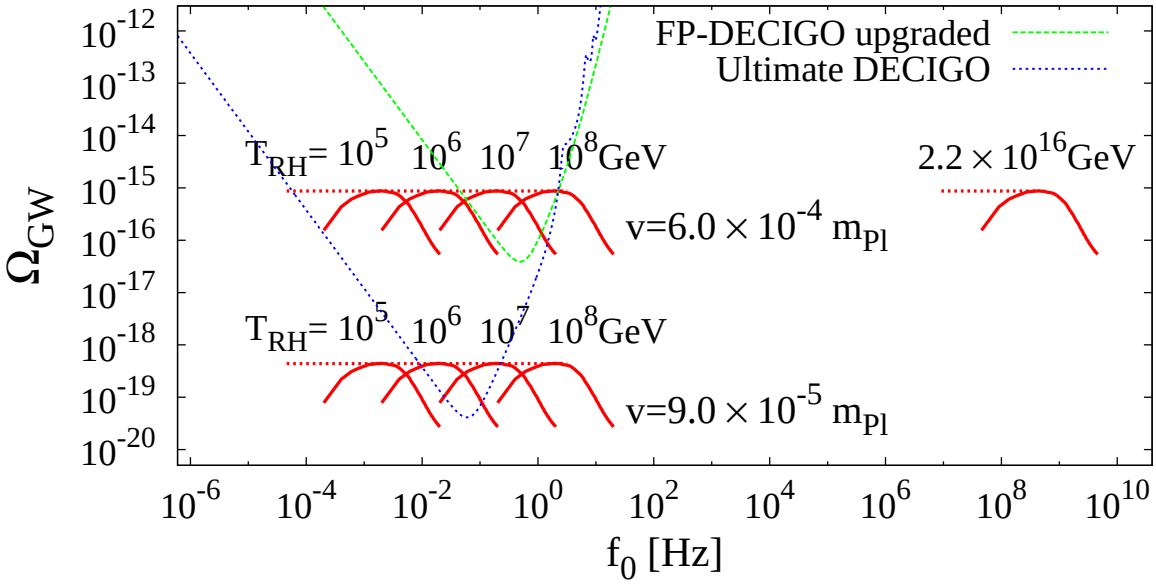

FIG. 5: Comparison with the sensitivity curves of future experiments. Gravitational wave spectra are plotted for different reheating temperatures and different values of v with $g_* = 106.75$. Here we use the result of $N = 4$.

with $x_{R'} = f/(1.7 f_R)$. Note the factor 1.7 in front of f_R in the definition of $x_{R'}$ represents the difference in the position of the spectral bend. If we tried to determine the reheating temperature by the spectral bend without knowing the origin of gravitational waves, we might make a wrong measurement deviated from the true value by 70%. Note also that the coefficient of the second term in the transfer function is changed from 0.22 to 0.6, which is a parameter to determine the sharpness of the spectral transition[2]. In Fig. 4, we also show the comparison between the simulation results and the spectra generated using the fitting formula.

D. Detectability in future experiments

Let us discuss the detectability of the reheating signature by future direct detection experiments. So far, we have shown the case with an unrealistically high reheating temperature $T_{\rm RH} = 2.2 \times 10^{16}$GeV due to the limitation of the simulation time and resolution. For lower reheating temperatures, although we cannot follow the whole evolution of the scalar field from the phase transition to the completion of reheating, the gravitational wave spectrum can be rescaled by just changing the frequency by $f_0 \propto g_*^{1/6} T_{\rm RH}$ for different reheating temperatures [37, 40]. Also, for different values of vacuum expectation value of the scalar field, the amplitude scales as $\Omega_{\rm GW} \propto v^4$ [19, 25].

Using the dependence on $T_{\rm RH}$ and v, we show the spectra for different reheating temperatures and different vacuum expectation values in Fig. 5, comparing with the sensitivity curves of the future satellite-type experiments such as DECIGO [7], BBO [8] and Ultimate DECIGO [6] (calculated assuming 10-year observation time). The noise curve titled as FP-DECIGO (Fabry-Pérot-type DECIGO) is the upgraded version from the original FP-DECIGO, whose sensitivity is improved about three times to remove all the foreground contamination from neutron star binaries [50]. Ultimate-DECIGO is the experiment which has the ideal sensitivity limited only by quantum noises.

In Fig. 6, we show how accurately the reheating temperature can be determined when the spectral shape of reheating is measured by the future experiments. We calculate Fisher matrices using the parameterization of Eq. (28) and estimate the expected errors on both $\Omega_{\rm GW,A}$ and $T_{\rm RH}$ assuming the noise designs of FP-DECIGO and Ultimate-DECIGO. In the calculation, we do not use the information in $f < 0.1$Hz, which may be contaminated by foreground

[2] Strictly speaking, the transfer function has a weak dependence on N. For example, this parameter takes 0.6 for $N = 4$ but is closer to 0.7 for $N = 8$.

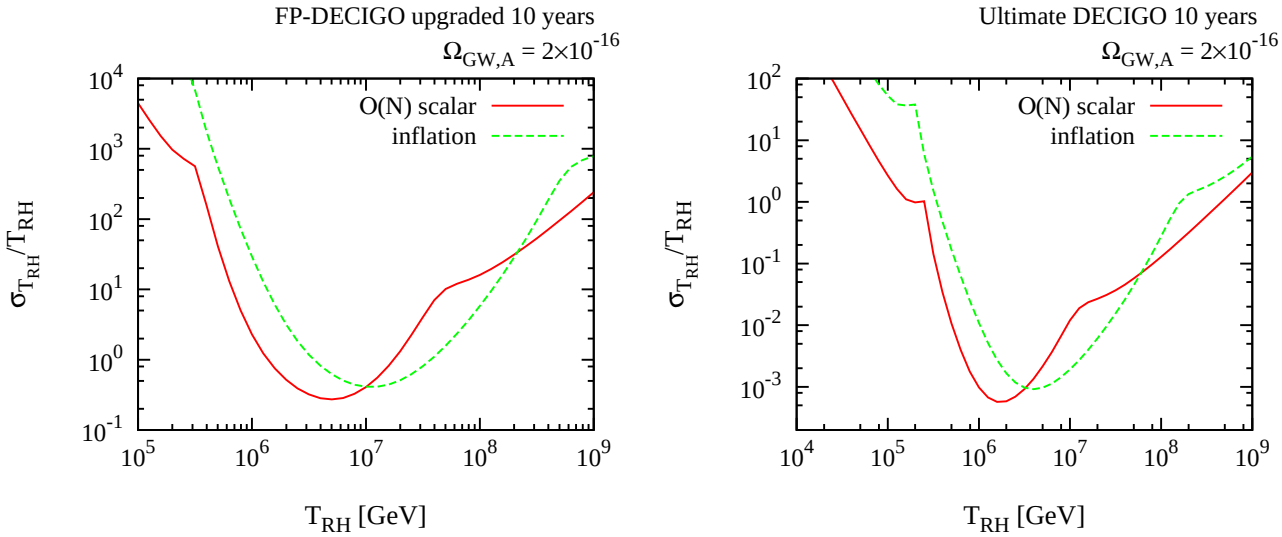

FIG. 6: The marginalized 1σ uncertainty in $T_{\rm RH}$ as a function of $T_{\rm RH}$ for upgraded FP-DECIGO (left panel) and Ultimate DECIGO (right panel). The red solid line represents the case of $O(N)$ phase transition and the green dashed line shows the case of inflation. The case with $\Omega_{\rm GW,A} = 2\times10^{-16}$ at the plateau region is shown for illustration, but the vertical axis simply scales as $\sigma_{T_{\rm RH}} \propto \Omega_{\rm GW,A}^{-1}$.

noise from white dwarf binaries. For the details of the calculation method of the Fisher matrix and the noise curves, see Ref. [51].

The curves shown in the figures are the 1σ errors on $T_{\rm RH}$ marginalized over the other parameter $\Omega_{\rm GW,A}$. Within the range of $T_{\rm RH}$ where $\sigma_{T_{\rm RH}}/T_{\rm RH} < 1$, one may expect that the reheating temperature can be determined with a certain level of accuracy. We also show the case of inflation for comparison. For inflationary gravitational waves, we find that FP-DECIGO is the most sensitive at $T_{\rm RH} \sim 10^7$GeV, [3] while it has a better sensitivity at slightly lower reheating temperature in the case of the $O(N)$ phase transition. This is because the position of the spectral bend is different depending on the origin, as has been seen in Fig. 4. This difference would cause an overestimate/underestimate of the reheating temperature by a factor of 1.7, if one estimates the reheating temperature with assuming an incorrect origin of the gravitational wave background.

Finally, we discuss whether it is possible to distinguish the gravitational wave background of the $O(N)$ phase transition from that of inflation. As seen in Eqs. (29) and (30), both of the transfer functions have the form of $T^2(x_R) = (1 - Bx_R^{1.5} + 0.65x_R^2)^{-1}$. The difference of origin arises in the coefficient of the second term B, which is 0.22 for inflation and about 0.6 for $O(N)$ phase transition. Therefore this parameter may help us to identify the origin of the observed gravitational waves if the value is precisely measured. Here, we perform the Fisher analysis by adding B as an additional free parameter. In Fig. 7, we show the expected 1σ error on B marginalized over $\Omega_{\rm GW,A}$ and $T_{\rm RH}$. The fiducial value of B is taken as 0.6. We see the error on B becomes smaller for larger normalization amplitude $\Omega_{\rm GW,A}$, because it corresponds to signal detection with a high signal-to-noise ratio. Since we need to measure the difference between $B = 0.22$ and 0.6, we may expect to specify the origin if B is determined with the accuracy of $\sigma_B < 0.1$. To achieve this accuracy, in the case where the reheating temperature is $T_{\rm RH} = 10^7$GeV, the amplitude of the gravitational wave should be larger than $\Omega_{\rm GW,A} = 8\times10^{-15}$ for FP-DECIGO, and $\Omega_{\rm GW,A} = 6\times10^{-18}$ for Ultimate DECIGO.

[3] Note that the sensitive frequency range for inflation is slightly different from the results in Ref. [51]. This is because we assume different value of g_* and also because we neglect the tilt of the spectrum in this paper.

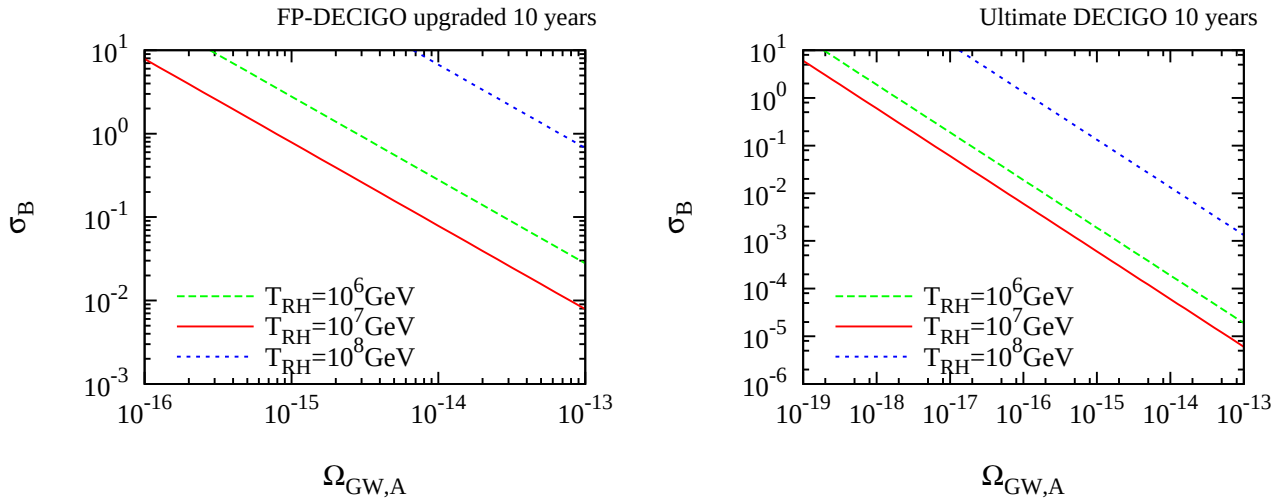

FIG. 7: The marginalized 1σ uncertainty in the coefficient of the second term in the transfer function B, which would enable us to discriminate the origin of the gravitational wave background if $\sigma_B < 0.1$. We show the result as a function of the normalization amplitude $\Omega_{\rm GW,A}$ for upgraded FP-DECIGO (left panel) and Ultimate DECIGO (right panel). Three lines represent different fiducial values of $T_{\rm RH}$.

IV. CONCLUSION

We have investigated how the effect of reheating appears in the gravitational wave background spectrum of the global $O(N)$ phase transition. Using numerical lattice simulations, we showed the power-law dependence of the spectrum changes from f^{-2} to f^0, which is an imprint of the change of the Hubble expansion rate from inflaton-oscillation dominated to radiation dominated regimes at the end of reheating. We also compared our result with the spectrum of inflation-produced gravitational waves and found differences in the position of the reheating signature and in the shape of the spectrum. By introducing a fitting function of the spectral shape, we performed a Fisher analysis to discuss whether one can determine the reheating temperature by detecting the gravitational waves from the $O(N)$ phase transition with future experiments. We have also investigated whether one can distinguish the origin between $O(N)$ phase transition and inflation by detecting the small difference in the spectral shape alone.

Observation of gravitational wave provides a unique opportunity to probe the very early epoch of the Universe. Inflation is one of the strong candidates as a generation mechanism of gravitational waves in the early Universe, which could be used as a tool to extract information on the thermal history after inflation. At the same time, we should always keep in mind that there may be alternative ways to probe it using gravitational waves from different origins. The change of the Hubble expansion rate in general affects the evolution of gravitational waves through the Hubble expansion term in the evolution equation. Gravitational waves from a global $O(N)$ phase transition is a good example which clearly contains the effect in its scale-invariant spectrum. Although this paper has focused on the effect under the background of the conventional reheating model, it could be used to test any type of mechanism in the early Universe which induces a different behavior of the Hubble expansion rate.

Acknowledgments

This work is partly supported by Career Development Project for Researchers of Allied Universities (SK). This work was partially supported by JSPS KAKENHI Grant Numbers 23340058(JY) and 15H02082. This work was supported in part by MEXT SPIRE and JICFuS (TH).

[1] G. M. Harry [LIGO Scientific Collaboration], Class. Quant. Grav. **27**, 084006 (2010).

[2] T. Accadia, F. Acernese, F. Antonucci, P. Astone, G. Ballardin, F. Barone, M. Barsuglia and A. Basti *et al.*, Class. Quant. Grav. **28**, 114002 (2011).
[3] K. Somiya [KAGRA Collaboration], Class. Quant. Grav. **29**, 124007 (2012) [arXiv:1111.7185 [gr-qc]].
[4] P. Amaro-Seoane, S. Aoudia, S. Babak, P. Binetruy, E. Berti, A. Bohe, C. Caprini and M. Colpi *et al.*, arXiv:1201.3621 [astro-ph.CO].
[5] P. Amaro-Seoane, S. Aoudia, S. Babak, P. Binetruy, E. Berti, A. Bohe, C. Caprini and M. Colpi *et al.*, Class. Quant. Grav. **29**, 124016 (2012) [arXiv:1202.0839 [gr-qc]].
[6] N. Seto, S. Kawamura and T. Nakamura, Phys. Rev. Lett. **87**, 221103 (2001) [astro-ph/0108011].
[7] S. Kawamura, M. Ando, N. Seto, S. Sato, T. Nakamura, K. Tsubono, N. Kanda and T. Tanaka *et al.*, Class. Quant. Grav. **28**, 094011 (2011).
[8] S. Phinney *et al.*, *The big bang observer: direct detection of gravitational waves from the birth of the Universe to the present*, NASA Mission Concept Study.
[9] L. M. Krauss, Phys. Lett. B **284**, 229 (1992).
[10] M. Kamionkowski, A. Kosowsky and A. Stebbins, Phys. Rev. Lett. **78**, 2058 (1997) [astro-ph/9609132].
[11] M. Zaldarriaga and U. Seljak, Phys. Rev. D **55**, 1830 (1997) [astro-ph/9609170].
[12] J. Tauber *et al.* [Planck Collaboration], astro-ph/0604069.
[13] D. Hanson *et al.* [SPTpol Collaboration], Phys. Rev. Lett. **111**, 141301 (2013) [arXiv:1307.5830 [astro-ph.CO]].
[14] P. A. R. Ade *et al.* [The POLARBEAR Collaboration], arXiv:1403.2369 [astro-ph.CO].
[15] G. Hobbs, A. Archibald, Z. Arzoumanian, D. Backer, M. Bailes, N. D. R. Bhat, M. Burgay and S. Burke-Spolaor *et al.*, Class. Quant. Grav. **27**, 084013 (2010) [arXiv:0911.5206 [astro-ph.SR]].
[16] R. van Haasteren, Y. Levin, G. H. Janssen, K. Lazaridis, M. Kramer, B. W. Stappers, G. Desvignes and M. B. Purver *et al.*, Mon. Not. Roy. Astron. Soc. **414**, no. 4, 3117 (2011) [Erratum-ibid. **425**, no. 2, 1597 (2012)] [arXiv:1103.0576 [astro-ph.CO]].
[17] P. B. Demorest, R. D. Ferdman, M. E. Gonzalez, D. Nice, S. Ransom, I. H. Stairs, Z. Arzoumanian and A. Brazier *et al.*, Astrophys. J. **762**, 94 (2013) [arXiv:1201.6641 [astro-ph.CO]].
[18] R. N. Manchester, G. Hobbs, M. Bailes, W. A. Coles, W. van Straten, M. J. Keith, R. M. Shannon and N. D. R. Bhat *et al.*, arXiv:1210.6130 [astro-ph.IM].
[19] K. Jones-Smith, L. M. Krauss and H. Mathur, Phys. Rev. Lett. **100**, 131302 (2008) [arXiv:0712.0778 [astro-ph]].
[20] E. Fenu, D. G. Figueroa, R. Durrer and J. Garcia-Bellido, JCAP **0910**, 005 (2009) [arXiv:0908.0425 [astro-ph.CO]].
[21] J. T. Giblin, Jr., L. R. Price, X. Siemens and B. Vlcek, JCAP **1211**, 006 (2012) [arXiv:1111.4014 [astro-ph.CO]].
[22] D. G. Figueroa, M. Hindmarsh and J. Urrestilla, Phys. Rev. Lett. **110**, no. 10, 101302 (2013) [arXiv:1212.5458 [astro-ph.CO]].
[23] R. Durrer, M. Kunz and A. Melchiorri, Phys. Rev. D **59**, 123005 (1999) [astro-ph/9811174].
[24] J. Garcia-Bellido, R. Durrer, E. Fenu, D. G. Figueroa and M. Kunz, Phys. Lett. B **695**, 26 (2011) [arXiv:1003.0299 [astro-ph.CO]].
[25] E. Fenu, D. G. Figueroa, R. Durrer, J. Garcia-Bellido and M. Kunz, arXiv:1311.3225 [astro-ph.CO].
[26] P. Adshead and E. A. Lim, Phys. Rev. D **82**, 024023 (2010) [arXiv:0912.1615 [astro-ph.CO]].
[27] D. G. Figueroa, R. R. Caldwell and M. Kamionkowski, Phys. Rev. D **81**, 123504 (2010) [arXiv:1003.0672 [astro-ph.CO]].
[28] M. A. Amin and D. Grin, arXiv:1405.1039 [astro-ph.CO].
[29] D. Baumann and M. Zaldarriaga, JCAP **0906**, 013 (2009) [arXiv:0901.0958 [astro-ph.CO]].
[30] P. Adshead and E. A. Lim, Phys. Rev. D **82**, 024023 (2010) [arXiv:0912.1615 [astro-ph.CO]].
[31] L. M. Krauss, K. Jones-Smith, H. Mathur and J. Dent, Phys. Rev. D **82**, 044001 (2010) [arXiv:1003.1735 [astro-ph.CO]].
[32] P. A. R. Ade *et al.* [Planck Collaboration], Astron. Astrophys. **571**, A25 (2014) [arXiv:1303.5085 [astro-ph.CO]].
[33] J. Urrestilla, N. Bevis, M. Hindmarsh, M. Kunz and A. R. Liddle, JCAP **0807**, 010 (2008) [arXiv:0711.1842 [astro-ph]].
[34] J. B. Dent, L. M. Krauss and H. Mathur, arXiv:1403.5166 [astro-ph.CO].
[35] R. Durrer, D. G. Figueroa and M. Kunz, arXiv:1404.3855 [astro-ph.CO].
[36] J. Lizarraga, J. Urrestilla, D. Daverio, M. Hindmarsh, M. Kunz and A. R. Liddle, Phys. Rev. D **90**, no. 10, 103504 (2014) [arXiv:1408.4126 [astro-ph.CO]].
[37] N. Seto and J. Yokoyama, J. Phys. Soc. Jap. **72**, 3082 (2003) [gr-qc/0305096].
[38] L. A. Boyle and P. J. Steinhardt, Phys. Rev. D **77**, 063504 (2008) [astro-ph/0512014].
[39] K. Nakayama, S. Saito, Y. Suwa and J. Yokoyama, Phys. Rev. D **77**, 124001 (2008) [arXiv:0802.2452 [hep-ph]];
[40] K. Nakayama, S. Saito, Y. Suwa and J. Yokoyama, JCAP **0806**, 020 (2008) [arXiv:0804.1827 [astro-ph]].
[41] K. Nakayama and J. Yokoyama, JCAP **1001**, 010 (2010) [arXiv:0910.0715 [astro-ph.CO]].
[42] S. Kuroyanagi, T. Chiba and N. Sugiyama, Phys. Rev. D **83**, 043514 (2011) [arXiv:1010.5246 [astro-ph.CO]].
[43] S. Kuroyanagi, K. Nakayama and S. Saito, Phys. Rev. D **84**, 123513 (2011) [arXiv:1110.4169 [astro-ph.CO]].
[44] S. Kuroyanagi, C. Ringeval and T. Takahashi, Phys. Rev. D **87**, 083502 (2013) [arXiv:1301.1778 [astro-ph.CO]].
[45] M. Yamaguchi, Phys. Rev. D **60** (1999) 103511 [hep-ph/9907506].
[46] T. Hiramatsu, M. Kawasaki and K. 'i. Saikawa, JCAP **1005**, 032 (2010) [arXiv:1002.1555 [astro-ph.CO]].
[47] J. F. Dufaux, A. Bergman, G. N. Felder, L. Kofman and J. -P. Uzan, Phys. Rev. D **76**, 123517 (2007) [arXiv:0707.0875 [astro-ph]].
[48] T. Kobayashi, M. Yamaguchi and J. Yokoyama, JCAP **1507**, no. 07, 017 (2015) [arXiv:1504.05710 [hep-th]].
[49] S. Kuroyanagi, T. Takahashi and S. Yokoyama, arXiv:1407.4785 [astro-ph.CO].
[50] K. Yagi and N. Seto, Phys. Rev. D **83**, 044011 (2011) [arXiv:1101.3940 [astro-ph.CO]].
[51] S. Kuroyanagi, K. Nakayama and J. Yokoyama, PTEP **2015**, no. 1, 013E02 (2015) [arXiv:1410.6618 [astro-ph.CO]].